ELSEVIER

The local microscale problem in the multiscale modeling of strongly heterogeneous media: Effects of boundary conditions and cell size

Xingye Yue [a,*], Weinan E [b]

[a] *Department of Mathematics, Suzhou University, Suzhou 215006, China*
[b] *Department of Mathematics and PACM, Princeton University, NJ 08544, USA*

Abstract

Many multiscale methods are based on the idea of extracting macroscopic behavior of solutions by solving an array of microscale models over small domains. A key ingredient in such multiscale methods is the boundary condition and the size of the computational domain over which the microscale problems are solved. This problem is systematically investigated in the present paper in the context of modeling strongly heterogeneous media. Three different boundary conditions are considered: the periodic boundary condition, Dirichlet boundary condition, and the Neumann boundary condition. Each is applied to several benchmark problems: the random checker-board problem, periodic problem with isotropic macroscale behavior, periodic problem with anisotropic macroscale behavior and periodic laminated media. In each case, convergence studies are conducted as the domain size for the microscale problem is changed. Convergence rates as well as the size of fluctuations in the computed effective coefficients are compared for the different formulations. In addition, we will discuss a mixed Dirichlet–Neumann boundary condition that is often used in porous medium modeling. We explain why that leads to unsatisfactory results and how it can be corrected. Also discussed are the different averaging methods used in extracting the effective coefficients.
© 2006 Elsevier Inc. All rights reserved.

1. Introduction

A central theme in many multiscale methods is to capture the macroscopic behavior of the solutions by solving an array of the microscale models locally over small computational domains. The microscale problems might be solved in a preprocessing step, in which case effective parameters or macroscale models are extracted

---

* Corresponding author. Present address: Department of Mathematics, University of Science and Technology of China, Hefei 230026, China.
    E-mail addresses: xyyue@ustc.edu.cn (X. Yue), weinan@math.princeton.edu (W. E).

which are then used in the computation of the macroscale solutions. Alternatively the microscale problems can be solved "on-the-fly" as the macroscale computation proceeds, in a concurrent coupling framework [1]. In any case, a key ingredient in such methods is the formulation, particularly the boundary conditions, of the microscale model, and the size of the computational domains over which the microscale problem is solved. Clearly from the viewpoint of efficiency, we would like these domains to be as small as possible. However, accuracy requirement often points to the opposite direction. Crucial to both accuracy and efficiency are the boundary conditions that we impose on the microscale problems. These boundary conditions are in some sense artificial – they are required only because the computational domains are truncated and localized.

The present paper addresses this issue for a specific problem: transport in a strongly heterogeneous medium described by:

$$-\nabla \cdot (k^{\varepsilon}(\mathbf{x})\nabla u^{\varepsilon}(\mathbf{x})) = f(\mathbf{x}), \quad \mathbf{x} \in \Omega \subset \mathbb{R}^{d}. \tag{1.1}$$

Here, ε is a small parameter that signifies explicitly the multiscale nature of the coefficient $k^{\varepsilon}(\mathbf{x})$, which will be referred to as the conductivity tensor. Our aim is to study the accuracy with which the effective macroscale conductivity tensor is approximated by solving the local microscale problems with certain boundary conditions as the domain size varies.

Studies of this type have been reported in the literature. Pecullan et al. considered a similar problem for the elastic properties of periodic and hierarchical two-dimensional composites in [9]. Durlofsky [4] has studied the problem of extracting effective permeability of a porous medium by solving the microscale Darcy's law on a representative volume and considered the effects of different boundary conditions. In particular, he demonstrated that an often used mixed Dirichlet–Neumann boundary condition may give rather unsatisfactory results in some cases.We will discuss four examples. The first is a random checker-board problem. This is a nice example since its effective parameters can be computed exactly. Then we consider three examples of periodic microstructure with different macroscopic properties: isotropic, anisotropic, and laminated. From our results we conclude that while all three boundary conditions considered perform reasonably well, the periodic boundary condition gives the best results. Our results also demonstrate the clear advantage of the systematic procedures embodied in the heterogeneous multiscale method (HMM) [5], with which the difficulties observed by Durlofsky are automatically avoided.

2. Formulation of the microscale problems

2.1. Review of HMM

To be concrete, we will work in the framework of the heterogeneous multiscale method (HMM) which is a general framework for designing multiscale methods by coupling together solutions of local microscale problems [5]. The model input for HMM is the microscale model and a guess of how the macroscale model might be like. The output is the macroscale behavior of the solutions as well as samples of the local microstructure, e.g. typical microstructure near defects. Note that it is not the purpose of HMM to resolve the microscale behavior everywhere – that would require solving the microscale problem over the whole computational domain. On the other hand HMM does probe the local microstructure in a statistical sense, and if necessary, one can improve the accuracy for the local microstructure through post-processing.

There are two main components in the heterogeneous multiscale method: (1) an overall macroscopic scheme for the macroscale variables on a macroscale grid and (2) estimating the missing macroscopic data from the microscopic model. For (1.1), the macroscopic solver can be chosen simply as the standard C^{0} piecewise linear finite element method over a macroscopic triangulation $\mathcal{T}_{H}$ of mesh size H. We will denote by X_{H} the macroscopic finite element space which could be the standard piecewise linear finite elements over T_{H}. The data that need to be estimated from the microscale model is the stiffness matrix on $\mathcal{T}_{H}$: $A = (A_{ij})$, where

$$A_{ij} = \int_{\Omega} \nabla \Phi_{i}(\mathbf{x}) K_{H}(\mathbf{x}) \nabla \Phi_{j}(\mathbf{x}) \mathrm{d}\mathbf{x}. \tag{2.1}$$

Here, $K_{H}(\mathbf{x})$ is the effective conductivity at scale H and $\{\Phi_{i}(\mathbf{x})\}$ are the basis functions for X_{H}. Had we known $K_{H}(\mathbf{x})$, we could have evaluated A_{ij} simply by numerical quadrature: let $f_{ij}(\mathbf{x}) = \nabla \Phi_{i}(\mathbf{x}) K_{H}(\mathbf{x}) \nabla \Phi_{j}(\mathbf{x})$, then

$$A_{ij} = \int_{\Omega} f_{ij}(\mathbf{x})\mathrm{d}\mathbf{x} \simeq \sum_{T \in \mathcal{T}_H} |T| \sum_{\mathbf{x}_k \in T} \omega_k f_{ij}(\mathbf{x}_k),$$ (2.2)

where $\{\mathbf{x}_k\}$ and $\{\omega_k\}$ are the quadrature points and weights, respectively $|T|$ is the volume of the element $|T|$.

In the absence of explicit knowledge of $K_H(\mathbf{x})$, our problem reduces to the approximation of the values of $\{K_H(\mathbf{x}_k)\}$. This will be done by solving the original microscale model locally around each quadrature point $\{\mathbf{x}_k\}$ (see Fig. 1).

Let $I_\delta(\mathbf{x}_k) \ni \mathbf{x}_k$ be a cube of size δ. Consider

$$\nabla \cdot (k^\varepsilon(\mathbf{x}) \nabla \phi^\varepsilon) = 0, \quad \mathbf{x} \in I_\delta(\mathbf{x}_k).$$ (2.3)

The boundary condition for this problem is the main topic discussed below. The main objective is to probe efficiently the microscale behavior under the constraint that the average gradient of the solution ϕ^ε is fixed to be a given constant vector. Having the solution to this local problem, we can define the effective conductivity tensor at $\mathbf{x}_k$ by the relation

$$\langle k^\varepsilon(\mathbf{x}) \nabla \phi^\varepsilon \rangle_{I_\delta} = K_H(\mathbf{x}_k) \langle \nabla \phi^\varepsilon \rangle_{I_\delta},$$ (2.4)

where $\langle v \rangle_{I_\delta} = \frac{1}{|I_\delta|} \int_{I_\delta} v \, \mathrm{d}\mathbf{x}$. The basis of this procedure is the homogenization theorem which has been proved in various contexts; the most general result is found in [8]. The homogenization theorems allow us to define the effective (or homogenized) conductivity tensor, by considering the infinite volume limit of the solutions of the microscale problem subject to the constraint that the average gradient remains fixed. The effective tensor is defined by an average relation of the type (2.4) in the infinite volume limit, i.e.

$$L = \frac{\delta}{\varepsilon} \to \infty.$$

In the special case when the microstructure is periodic, the infinite volume problem reduces to a periodic problem and therefore can be considered on its period.

In practice, one solves (2.3) with the constraint $\langle \nabla \phi^\varepsilon \rangle_{I_\delta} = \mathbf{e}_1, \ldots, \mathbf{e}_d$, respectively, where d is the spatial dimension of the problem. Denote these solutions by ϕ_j^ε, $j = 1, \ldots, d$. Then

$$(\langle k^\varepsilon(\mathbf{x}) \nabla \phi_1^\varepsilon \rangle_{I_\delta}, \ldots, \langle k^\varepsilon(\mathbf{x}) \nabla \phi_d^\varepsilon \rangle_{I_\delta}) = K_H(\mathbf{x}_k).$$ (2.5)

In summary, the overall algorithm consists of the following steps:

- Solve for $\phi_1^\varepsilon, \ldots, \phi_\varepsilon^d$ using the boundary conditions discussed below, at each $\mathbf{x}_k$.
- Obtain the approximate values of $K_H(\mathbf{x}_k)$ by averaging the microscale solutions using (2.5).
- Assemble the effective stiffness matrix using (2.2).
- Solve the macroscale finite element equation using the effective stiffness matrix. If we express the macroscale solution in X_H in the form of $U_H(\mathbf{x}) = \sum U_j \Phi_j(\mathbf{x})$, then the macroscale finite element equation takes the standard form:
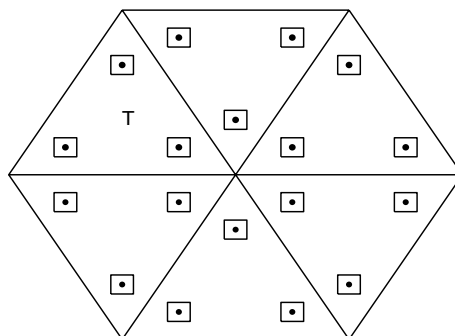

Fig. 1. Illustration of HMM for solving (1.1). The dots are the quadrature points in (2.2). The little squares are the microcell $I_\delta(\mathbf{x}_k)$.

$$AU = F, \tag{2.6}$$

where $U = (U_1, \ldots, U_N)^T$, $F = (F_1, \ldots, F_N)^T$, $F_j = (f(\mathbf{x}), \Phi_j(\mathbf{x}))$.

For the particular problem discussed here, HMM is clearly very closely related to solving homogenized equations with effective coefficients estimated numerically beforehand by solving the microscale problem. The difference is that HMM formulates the two components, estimating effective coefficients and solving the approximate homogenized problem, simultaneously instead of sequentially. For nonlinear problems, this difference seems quite crucial. In addition, HMM gives us quite naturally not only the macroscale information, but also samples of microstructural information. Of course, in the sequential approach one may also think of ways to make use of the microstructural information. But it seems less natural and as a result, this has not been explored much.

In any case, a key component for both strategies is to formulate the boundary conditions for the microscale problem. We now turn to this issue.

2.2. The local microscale problems

The local microscale problem is constrained by the local macroscopic state through the constraint:

$$\langle \nabla \phi^\varepsilon \rangle_{I_\delta} = G \tag{2.7}$$

for some fixed constant vector G. We will discuss the three natural boundary conditions: the periodic boundary condition, the Dirichlet boundary condition, and the Neumann boundary condition. With the exception of the Neumann boundary condition, these have been used in one way or another in the literature (see [4,11,12]). In [3], the author considered a kind of Neumann boundary condition, but it is quite different from what we discuss here [6].

2.2.1. Dirichlet formulation

In this case, Dirichlet boundary condition is used for the local microscale problem (2.3)

$$\phi^\varepsilon(\mathbf{x}) = G \cdot \mathbf{x}, \quad \text{on } \partial I_\delta. \tag{2.8}$$

2.2.2. Periodic formulation

The local microscale problem (2.3) is subject to the following boundary condition:

$$\phi^\varepsilon(\mathbf{x}) - G \cdot \mathbf{x} \text{ is periodic with period } I_\delta. \tag{2.9}$$

It can be checked easily that the constraint (2.7) is satisfied for both the Dirichlet and periodic formulation.

2.2.3. Neumann formulation

In this case, we have

$$k^\varepsilon(\mathbf{x}) \nabla \phi^\varepsilon(\mathbf{x}) \cdot \mathbf{n} = \lambda \cdot \mathbf{n}, \quad \text{on } \partial I_\delta, \tag{2.10}$$

where the constant vector $\lambda \in \mathbb{R}^d$ is the Lagrange multiplier for the constraint that (see [6])

$$\langle \nabla \phi^\varepsilon \rangle = G. \tag{2.11}$$

For example when $d = 2$, to solve problem (2.3) and (2.10) with the constraint (2.11), we first solve for u_1 and u_2 from

$$\begin{cases} -\nabla \cdot (k^\varepsilon(\mathbf{x}) \nabla u_i) = 0, & \text{in } I_\delta, \\ k^\varepsilon(\mathbf{x}) \nabla u_i(\mathbf{x}) \cdot \mathbf{n} = \mu_i \cdot \mathbf{n}, & \text{on } \partial I_\delta, \end{cases} \tag{2.12}$$

for $i = 1, 2$, where $\mu_1 = (1,0)^T$, $\mu_2 = (0,1)^T$. Then given an arbitrary G, the Lagrange multiplier $\lambda = (\lambda_1, \lambda_2)^T$ is determined by the linear equations

$$\lambda_1 \langle \nabla u_1 \rangle + \lambda_2 \langle \nabla u_2 \rangle = G \tag{2.13}$$

and the solution of (2.3), (2.10), and (2.11) is given by $\phi^\varepsilon = \lambda_1 u_1 + \lambda_2 u_2$.

From this discussion, it is clear that the difference in the computational complexity of solving the local microscale problem using the different formulations is comparable to that of solving standard Dirichlet, periodic and Neumann problems.

Having solved the microscale problem, we define the effective conductivity tensor by

$$\langle k^{\varepsilon}(\mathbf{x})\nabla\phi^{\varepsilon}\rangle = K^{*}\langle\nabla\phi^{\varepsilon}\rangle = K^{*}G. \tag{2.14}$$

For each of the three formulations, we obtain, respectively, K_{D}^{*}, K_{P}^{*}, and K_{N}^{*}.

When the microstructure is periodic, K_{P}^{*} will be exactly the homogenized conductivity tensor obtained in the homogenization theory ([13]) if I_{δ} is chosen to be an integer multiple of the period.

2.3. Relation between the three different effective tensors

Theorem 2.1. *For the three effective tensors, the following relation is valid*:

$$K_{\mathrm{N}}^{*} \leqslant K_{\mathrm{P}}^{*} \leqslant K_{\mathrm{D}}^{*}. \tag{2.15}$$

This explains the observation reported below that in general the Dirichlet formulation provides an overestimate for the effective conductivity tensor and the Neumann formulation provides an under-estimate.

It is easy to see that for the one-dimensional case, the three quantities are equal.

Proof of the theorem. We first note that the effective tensors have a variational formulation: For any $G \in \mathbb{R}^{d}$,

$$G^{\mathrm{T}}K_{\mathrm{D}}^{*}G = \min_{v(\mathbf{x})\in V_{\mathrm{D}}} \langle k^{\varepsilon}(\mathbf{x})\nabla v \cdot \nabla v\rangle, \tag{2.16}$$

$$G^{\mathrm{T}}K_{\mathrm{P}}^{*}G = \min_{v(\mathbf{x})\in V_{\mathrm{P}}} \langle k^{\varepsilon}(\mathbf{x})\nabla v \cdot \nabla v\rangle, \tag{2.17}$$

$$G^{\mathrm{T}}K_{\mathrm{N}}^{*}G = \min_{v(\mathbf{x})\in V_{\mathrm{N}}} \langle k^{\varepsilon}(\mathbf{x})\nabla v \cdot \nabla v\rangle, \tag{2.18}$$

where the spaces of admissible functions are:

$$V_{\mathrm{D}} = \{v(\mathbf{x}) \in H^{1}(I_{\delta}) : v(\mathbf{x}) = G \cdot \mathbf{x} \quad \text{on } \partial I_{\delta}\}, \tag{2.19}$$

$$V_{\mathrm{P}} = \{v(\mathbf{x}) \in H^{1}(\mathbb{R}^{d}) : v(\mathbf{x}) - G \cdot \mathbf{x} \text{ is periodic with period } I_{\delta}\}, \tag{2.20}$$

$$V_{\mathrm{N}} = \{v(\mathbf{x}) \in H^{1}(I_{\delta}) : \langle\nabla v\rangle = G\}. \tag{2.21}$$

It is easy to see that $V_{\mathrm{D}} \subset V_{\mathrm{P}} \subset V_{\mathrm{N}}$, and for one-dimensional problem, these spaces are the same up to constants. Hence (2.15) follows.

We next check the equivalence of the two definitions for the effective tensors. We only discuss the Neumann formulation. The argument for the other formulations are the same. Let $u(\mathbf{x})$ be the solution of the Neumann problem (2.3) and (2.10) with the constraint (2.11). Then $u(\mathbf{x})$ satisfies [6]

$$\int_{I_{\delta}} k^{\varepsilon}(\mathbf{x})\nabla u \cdot \nabla u\, \mathrm{d}\mathbf{x} = \min_{v(\mathbf{x})\in V_{\mathrm{N}}} \int_{I_{\delta}} k^{\varepsilon}(\mathbf{x})\nabla v \cdot \nabla v\, \mathrm{d}\mathbf{x}.$$

Assume that K_{N}^{*} is defined by (2.14). Then we have

$$\int_{I_{\delta}} G^{\mathrm{T}}K_{\mathrm{N}}^{*}G\, \mathrm{d}\mathbf{x} = \int_{I_{\delta}} k^{\varepsilon}(\mathbf{x})\nabla u \cdot G\, \mathrm{d}\mathbf{x} = \int_{I_{\delta}} k^{\varepsilon}(\mathbf{x})\nabla u \cdot \nabla u\, \mathrm{d}\mathbf{x} + \int_{I_{\delta}} k^{\varepsilon}(\mathbf{x})\nabla u \cdot \nabla(G \cdot \mathbf{x} - u)\, \mathrm{d}\mathbf{x}$$

and for the second term on the right-hand side, by Green's formula

$$\int_{I_{\delta}} k^{\varepsilon}(\mathbf{x})\nabla u \cdot \nabla(G \cdot \mathbf{x} - u)\, \mathrm{d}\mathbf{x} = -\int_{I_{\delta}} \nabla \cdot (k^{\varepsilon}(\mathbf{x})\nabla u)(G \cdot \mathbf{x} - u)\, \mathrm{d}\mathbf{x} + \int_{\partial I_{\delta}} k^{\varepsilon}(\mathbf{x})\nabla u \cdot \mathbf{n}(G \cdot \mathbf{x} - u)\, \mathrm{d}S$$

$$= \int_{\partial I_{\delta}} \lambda \cdot \mathbf{n}(G \cdot \mathbf{x} - u)\, \mathrm{d}S = \int_{I_{\delta}} \nabla \cdot (\lambda(G \cdot \mathbf{x} - u))\, \mathrm{d}S = \lambda \cdot \int_{I_{\delta}} (G - \nabla u)\, \mathrm{d}\mathbf{x} = 0.$$

This argument also works in the reversed direction. Therefore (2.18) follows. The proof is completed.   □

2.4. Alternative averaging methods

The effective conductivity tensor is obtained from the solutions of the microscale problem through averaging. In (2.14), *direct averaging* is used. To reduce the effect of the boundary conditions, other averaging methods can be introduced. For example, 'weighted averaging' methods were suggested in [6] with the idea that the weight function is smooth but vanishes at the boundary. One may also use the simple 'truncated averaging' methods, by averaging the microscale solution over an interior subset of the domain, and the region near the boundary is truncated (see [7]).

Weighted averaging: $\langle v \rangle_w = \frac{1}{|I_\delta|} \int_{I_\delta} w_\delta(\mathbf{x}) v(\mathbf{x}) d\mathbf{x}$, where the weight function $w_\delta(\mathbf{x})$ satisfying

$$\frac{1}{|I_\delta|} \int_{I_\delta} w_\delta(\mathbf{x}) d\mathbf{x} = 1, \tag{2.22}$$

where $w_\delta(\mathbf{x}) = \frac{1}{\delta^d} w\left(\frac{\mathbf{x}}{\delta}\right)$. In our numerical work presented below, we choose the weight function as $w(\mathbf{x}) = (1 - \cos(x_1))(1 - \cos(x_2))$.

Truncated average: $\langle v \rangle_t = \frac{1}{|I'_\delta|} \int_{I'_\delta} v(\mathbf{x}) d\mathbf{x}$, where $I'_\delta \subset I_\delta$. In general we choose $\delta' = \delta/2$.

3. Effects of boundary condition and cell size

In the following we only consider problems in $\mathbb{R}^2$, i.e. $d = 2$. We will study the effects of boundary conditions and cell size by performing systematic numerical experiments. We will consider two types of problems: the case when the microstructure is given by a random checker-board and the case when the microstructure is periodic.

3.1. Random checker-board

Random checker-board is a two-phase composite material constructed by partitioning space into uniform square cells, each of which is randomly designated as being in phase 1 or phase 2 with probability p_1 and $p_2 = 1 - p_1$, respectively. We will set $p_1 = p_2 = 0.5$. We will work with the microscale, i.e. we will set $\varepsilon = 1$. We choose this as a test problem since it has the following special feature: suppose phase 1 and phase 2 are isotropic materials with scalar conductivity k_1 and k_2. Then the effective properties of the composite material are also isotropic at the macro-scale, and the effective conductivity is $K^* = k^* \mathbf{I} = \sqrt{k_1 k_2} \mathbf{I}$. This result is a consequence of the duality relations proved by Keller [10].

In the computations reported below, we set $k_1 = 2$, $k_2 = 8$. Hence the effective conductivity tensor is $K^* = 4\mathbf{I}$. We solve the microscale problem with different formulations on domains of size $\delta = L * \varepsilon = L = 4, 6, \ldots$

We will monitor the following quantities:

- Effective conductivity computed from a particular realization ω of the checker-board:

  $$K^*_D(L) = K^*_D(\omega, L), \quad K^*_P(L) = K^*_P(\omega, L) \quad \text{and} \quad K^*_N(L) = K^*_N(\omega, L).$$

- Ensemble averaged effective conductivity:

  $$\bar{K}^*_D(L) = \mathbb{E}K^*_D(\omega, L), \quad \bar{K}^*_P(L) = \mathbb{E}K^*_P(\omega, L) \quad \text{and}$$
  $$\bar{K}^*_N(L) = \mathbb{E}K^*_N(\omega, L).$$

Here, and in the following $\mathbb{E}$ denotes ensemble average.

- Mean square deviation:

  $$\sigma^2_D(L) = \mathbb{E}(K^*_D - \bar{K}^*_D)^2, \quad \sigma^2_P(L) = \mathbb{E}(K^*_P - \bar{K}^*_P)^2 \quad \text{and}$$
  $$\sigma^2_N(L) = \mathbb{E}(K^*_N - \bar{K}^*_N)^2.$$

In Table 1, we present the results of the ensemble averaged effective conductivity obtained using different boundary conditions for different cell size L. These results are also plotted in Figs. 2–4. Two conclusions can be drawn from this. The first is that the error of the ensemble averaged effective conductivity behaves as
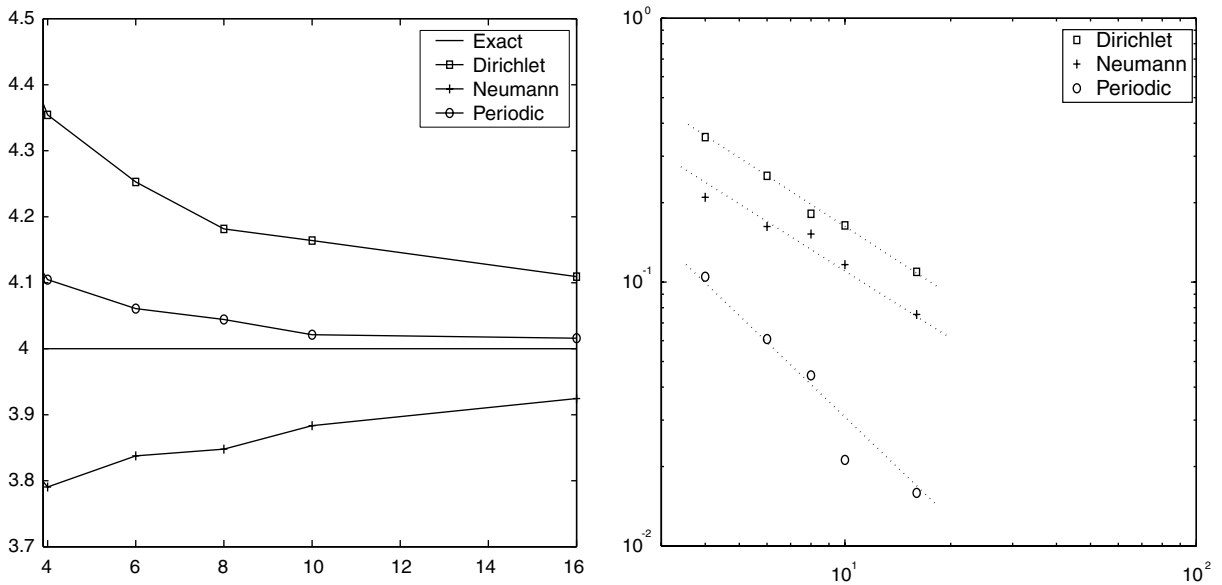
Table 1
Random checker-board – ensemble averaged effective conductivities computed using different boundary conditions

Cell size	4	6	8	10	16
Number of realizations	1000	800	800	400	100
$\bar{K}_D^*$	4.354	4.253	4.182	4.164	4.109
$\bar{K}_P^*$	4.105	4.061	4.044	4.021	4.016
$\bar{K}_N^*$	3.790	3.838	3.848	3.883	3.925
σ_D^2	0.619	0.295	0.153	0.090	0.035
σ_P^2	0.645	0.267	0.153	0.093	0.038
σ_N^2	0.502	0.204	0.134	0.080	0.030

Fig. 2. Random checker-board – ensemble averaged effective conductivities computed using different boundary conditions vs. the cell size (left); log–log plot of the absolute error vs. cell size (right): the slopes of the dotted lines for Dirichlet, Neumann, and periodic formulations are −0.85, −0.80, −1.50, respectively.

$$K^* - \bar{K}^*(L) \sim L^{-\alpha}$$

with α close to *1* for Dirichlet and Neumann formulations, and α close 1.5 for the periodic formulation. The second is that the periodic formulation performs better than the other formulations. This second conclusion is consistently observed in all of our numerical experiments.

Fig. 3 shows the behavior of the mean square deviation as a function of L. Again we have

$$\sigma^2 \sim L^{-\alpha}$$

with α close to 2 for all three formulations. This is consistent with the predictions of a naive application of the central limit theorem, which suggests

$$\sigma \sim N^{-1/2}$$

where $N \sim L^d$, d is the dimension. This statement can be proved easily for $d = 1$, and our numerical result suggests that this is also true for $d = 2$.

In Fig. 4, we present the histograms of 6000 realizations for $K^*(\omega, L)$ with $L = 4, 8$, and 16. From this result, we might expect that the rescaled distribution of $K^*(\omega, L)$ converges to a limit as $L \to \infty$.
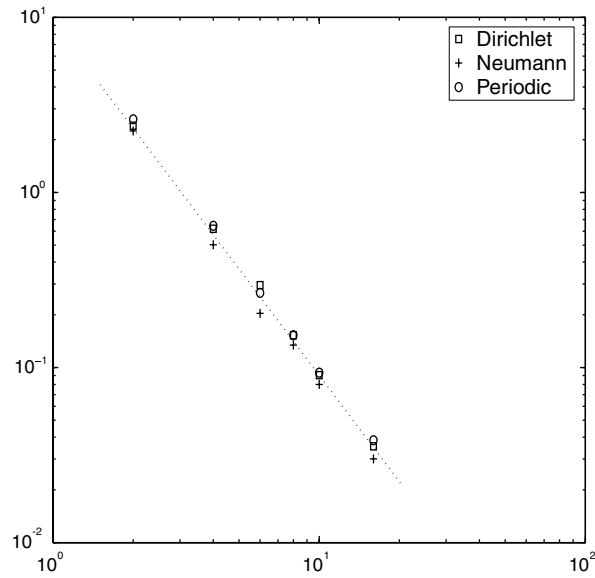
Fig. 3. Random checker-board – mean square deviation of the effective conductivities computed using different boundary conditions vs. the cell size. The slope of the dotted line is −2.03.

To see the behavior for some particular realizations, we first randomly construct a 32×32 checker-board, from which we select a subset of size $4 \times 4, \ldots, 32 \times 32$, respectively, such that the smaller ones are subsets of the bigger ones. Fig. 5 shows the results of two particular realizations. The results of the first realization are quite consistent with the behavior of the ensemble averages observed earlier. The results of the second realization, on the other hand, are quite different. This confirms that single realizations in random problems may not say much about typical behavior.

Next we turn to the case when the microstructure is periodic. We will discuss three cases. The first is when the macroscopic behavior is isotropic. The second is when the macroscopic behavior is anisotropic. The third is an example of laminated structure.

3.2. Periodic microstructure: isotropic in the macroscale

Consider the problem (1.1) with an isotropic conductivity tensor:

$$k^{\varepsilon}(\mathbf{x}) = \frac{1}{2 + 1.5\sin(2\pi x_1/\varepsilon)} * \frac{1}{2 + 1.5\sin(2\pi x_2/\varepsilon)} \mathbf{I}. \tag{3.1}$$

In this case the macroscopic effective conductivity tensor is isotropic: $K^* = k^*\mathbf{I} \simeq 0.3782\mathbf{I}$. As before, we denote by $K^*(L)$ the computed effective conductivity tensor by solving the microscale problem on a domain of size $\delta = L\varepsilon$. In Fig. 6, we show $K^*(L)$ as L changes. Also shown in Fig. 6 is the dependence of the error $|K^* - K^*(L)|$ on L for different formulations. Note that for the periodic formulation, the error is zero if L is an integer.

It is clear from Fig. 6 that the overall behavior in this case is very similar to that of Fig. 2. The Dirichlet and Neumann formulations give very similar results, and the periodic formulation gives better results.

Analogous to Fig. 3, we also show the behavior of the mean square deviation (or variance) $\sigma^2 = \sigma^2(L)$ in Fig. 7. This is done by uniformly distributing the domains over which the microscale problems are solved, and taking statistics with respect to the center of the domains. We see that $\sigma^2 \sim L^{-2}$. Unlike the random problem, this is expected to hold in all dimensions.

Figs. 3 and 7 suggest an interesting possibility, namely that for $d = 3$(three-dimensional problem), the variance decays faster for the random case than for the periodic case. It would be interesting to see if this is really true.
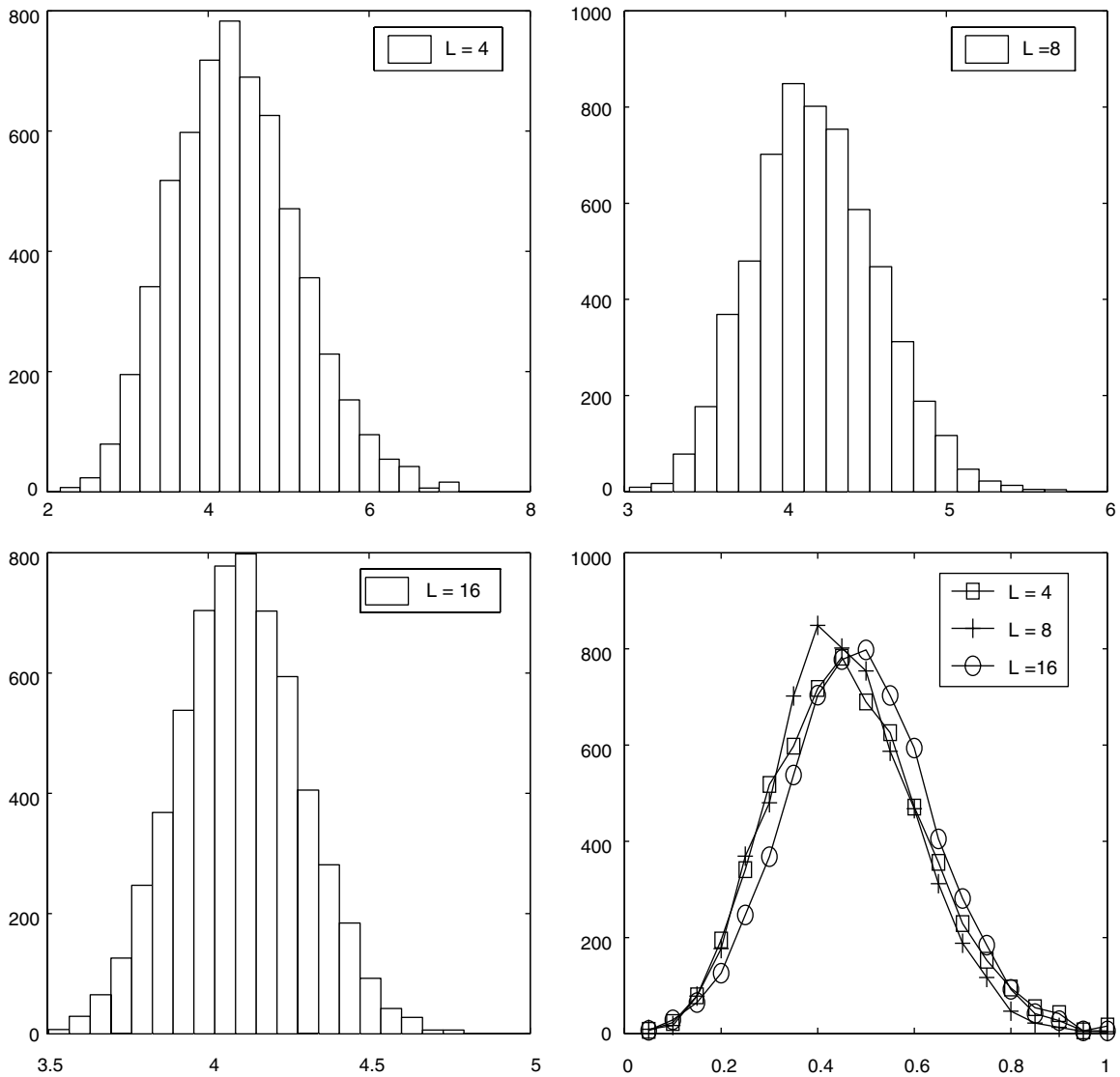
Fig. 4. Random checker-board – histograms of K_D^* for cell size of 4×4 (upper-left), 8×8 (upper-right), and 16×16 (lower-left) with 6000 realizations. The histograms are rescaled and depicted together in the lower-right figure. The behavior of K_P^* and K_N^* is similar.

Next we turn to an example for which the macroscopic effective tensor is anisotropic.

3.3. Periodic microstructure: anisotropic in the macroscale

We choose the coefficient in (1.1) as $k^\varepsilon(\mathbf{x})\mathbf{I}$ where

$$k^\varepsilon(\mathbf{x}) = \frac{2 + 1.5\sin(2\pi x_1/\varepsilon)}{2 + 1.5\sin(2\pi x_2/\varepsilon)} + \frac{2 + 1.5\sin(2\pi x_2/\varepsilon)}{2 + 1.5\cos(2\pi x_1/\varepsilon)}. \tag{3.2}$$

The effective coefficient tenser is given to high order accuracy by

$$K^* \simeq \begin{pmatrix} 2.3458 & 0 \\ 0 & 2.8746 \end{pmatrix}.$$
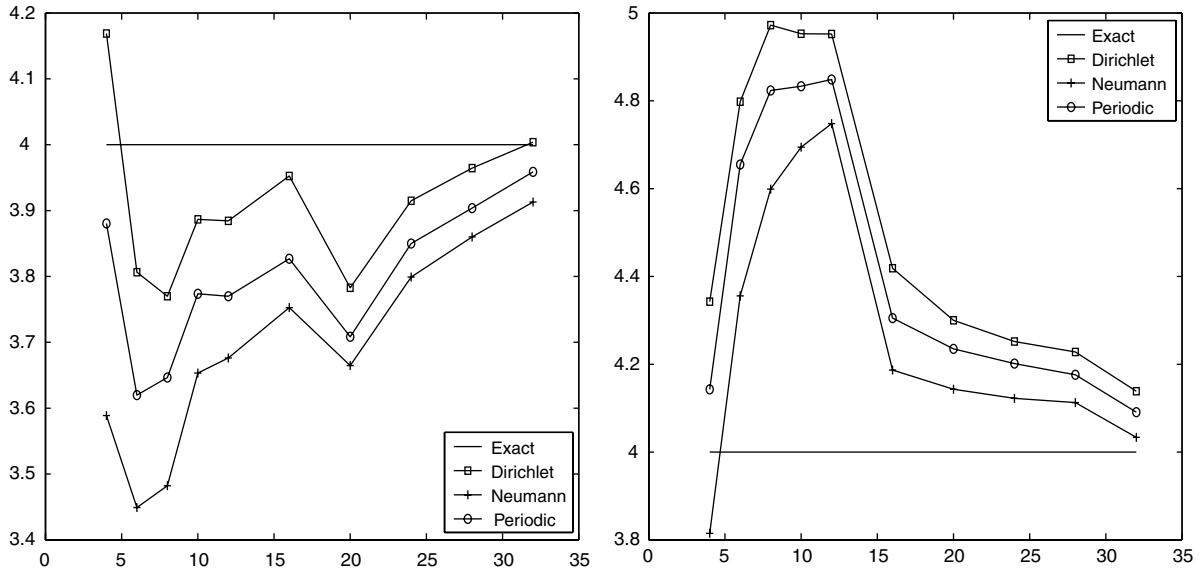
Fig. 5. Random checker-board – effective coefficient by different boundary conditions vs. local cell size for two special realizations.
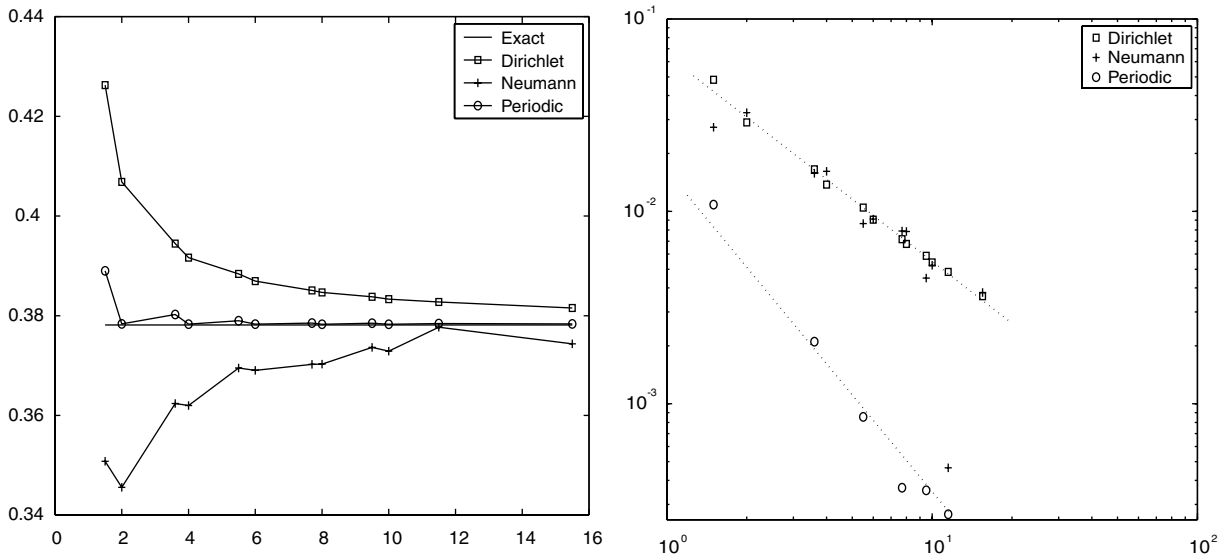
Fig. 6. Example (3.1) – effective conductivity tensor computed using different formulations vs. cell size (left) and the log–log plot of the error (right). The slope of the top dotted line in the right figure is -1.05, and the slope of the bottom dotted line is -1.50.

The results for this example are completely consistent with the results for the previous example. We only note one curious trend shown in Fig. 8, where we plot $|K^* - K^*(L)|$ for the two different components of the tensor. In this case $k_{11}^* < k_{22}^*$, and we see that the Neumann formulation does a better job approximating k_{11}^* and the Dirichlet formulation does a better job approximating k_{22}^*. This is consistent with our theoretical results in Theorem 2.1. Fig. 8 simply confirms what we would have expected based on previous results, namely that the periodic formulation does a better in general, with a slope bigger than 1; and the slopes for the other two formulations are close to 1.
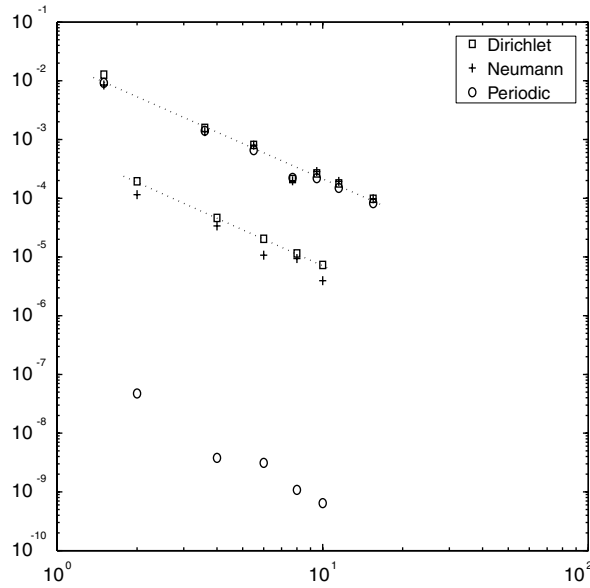
Fig. 7. Example (3.1) – mean square deviation vs. cell size L. The slope of the top dot line is -2.04 and the slope of the bottom one is -2.08.
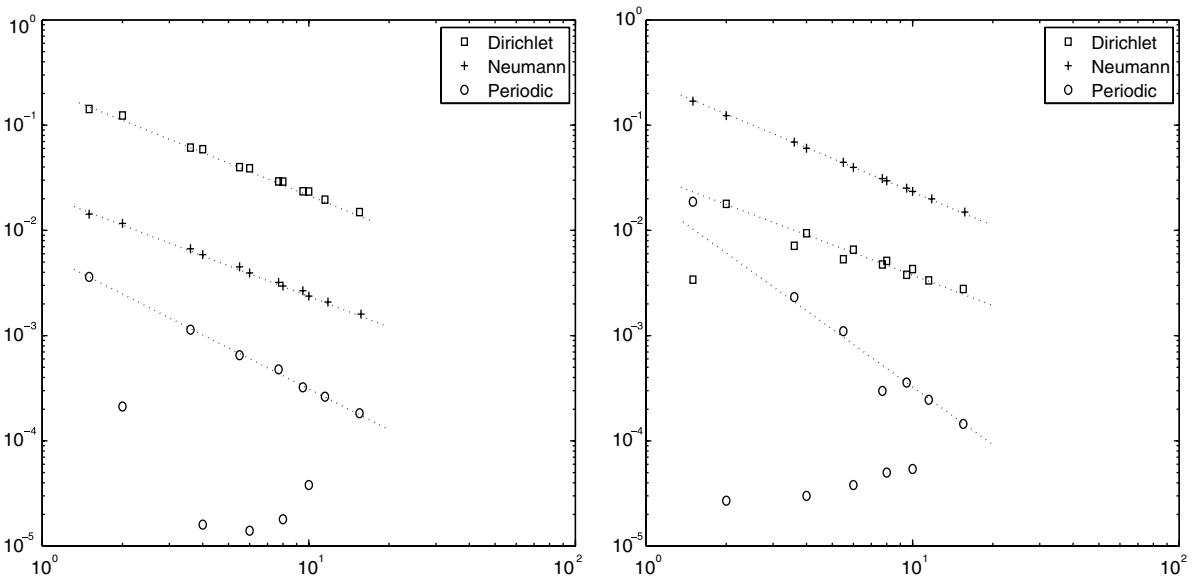

Fig. 8. Example (3.2) – error in the computed effective coefficient k_{11}^* (left) and k_{22}^* (right). The slopes of dotted lines in left figure from top to bottom are -0.97, -0.94, and -1.28; the slopes of dotted lines in the right figure from top to bottom are -1.04, -0.91, and -1.70.

3.4. Periodic laminated microstructure

Consider a layered medium (Durlofsky [4]) made up of two different materials, depicted in Fig. 9 (left), extended periodically over space. The thickness of material 1 is taken to be seven times that of material 2. The conductivity tensor of the two materials, denoted by $\mathbf{k}_1$ and $\mathbf{k}_2$, are as follows:
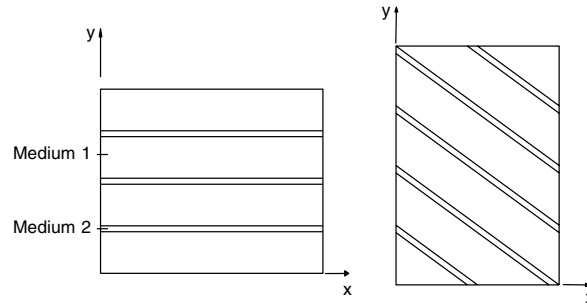
Fig. 9. Periodic laminated media.

$$\mathbf{k}_1 = \begin{pmatrix} 2 & 0 \\ 0 & 2 \end{pmatrix}, \quad \mathbf{k}_2 = \begin{pmatrix} 1 & 0 \\ 0 & 0.01 \end{pmatrix}.$$

The effective coefficient for the composite media can be obtained through weighted arithmetic (for k_{11}^*) and harmonic (for k_{22}^*) means as

$$K^* = \begin{pmatrix} 1.8750 & 0 \\ 0 & 0.0772947 \end{pmatrix}. \tag{3.3}$$

Next we rotate the layered medium relative to the coordinate axes by an angle of $-\frac{\pi}{4}$, as shown in Fig. 9 (right). The effective coefficient for the new system can be obtained by rotating the tensor in (3.3) by an angle of $-\frac{\pi}{4}$ ([2,4]):

$$K^* = \begin{pmatrix} 0.976147 & -0.898853 \\ -0.898853 & 0.976147 \end{pmatrix}. \tag{3.4}$$

This example was studied in [4]. We will focus on the rotated laminated system. Results are shown in Fig. 10. We see that they are completely consistent with the previous results.

In [4], the author considered a boundary condition which we will call *Dirichlet–Neumann* (D–N) boundary condition, i.e. Dirichlet boundary condition is used in one direction and no-flow boundary condition is used in the other direction. In D–N formulation, one needs to solve the following two local cell problems

$$\begin{cases} -\nabla \cdot (k^\varepsilon(\mathbf{x})\nabla u_1) = 0, & \text{in } I_\delta, \\ u_1(\mathbf{x}) = x_1, & \text{on left and right sides}, \\ k^\varepsilon(\mathbf{x})\nabla u_1 \cdot \mathbf{n} = 0, & \text{on top and bottom sides}, \end{cases} \tag{3.5}$$

and

$$\begin{cases} -\nabla \cdot (k^\varepsilon(\mathbf{x})\nabla u_2) = 0, & \text{in } I_\delta, \\ u_2(\mathbf{x}) = x_2, & \text{on top and bottom sides}, \\ k^\varepsilon(\mathbf{x})\nabla u_2 \cdot \mathbf{n} = 0, & \text{on left and right sides}. \end{cases} \tag{3.6}$$

The effective tensor K_{dn}^* is then determined by the following 4×4 system:

$$\langle k^\varepsilon(\mathbf{x})\nabla u_1 \rangle = K_{dn}^*(1,0)^{\mathrm{T}}, \tag{3.7}$$

$$\langle k^\varepsilon(\mathbf{x})\nabla u_2 \rangle = K_{dn}^*(0,1)^{\mathrm{T}}. \tag{3.8}$$

This procedure is often used in porous medium modeling. However, using this procedure, one obtained very unsatisfactory results: the effective tensor K_{dn}^* was diagonal with both diagonal elements equal to 0.193757.

The origin of this problem is quite simple. The D–N formulation does not impose the intended constraint in (2.7). For example, even though the x_1-gradient of u_1 is 1, the x_2-gradient is not 0, as we show in Table 2. If we
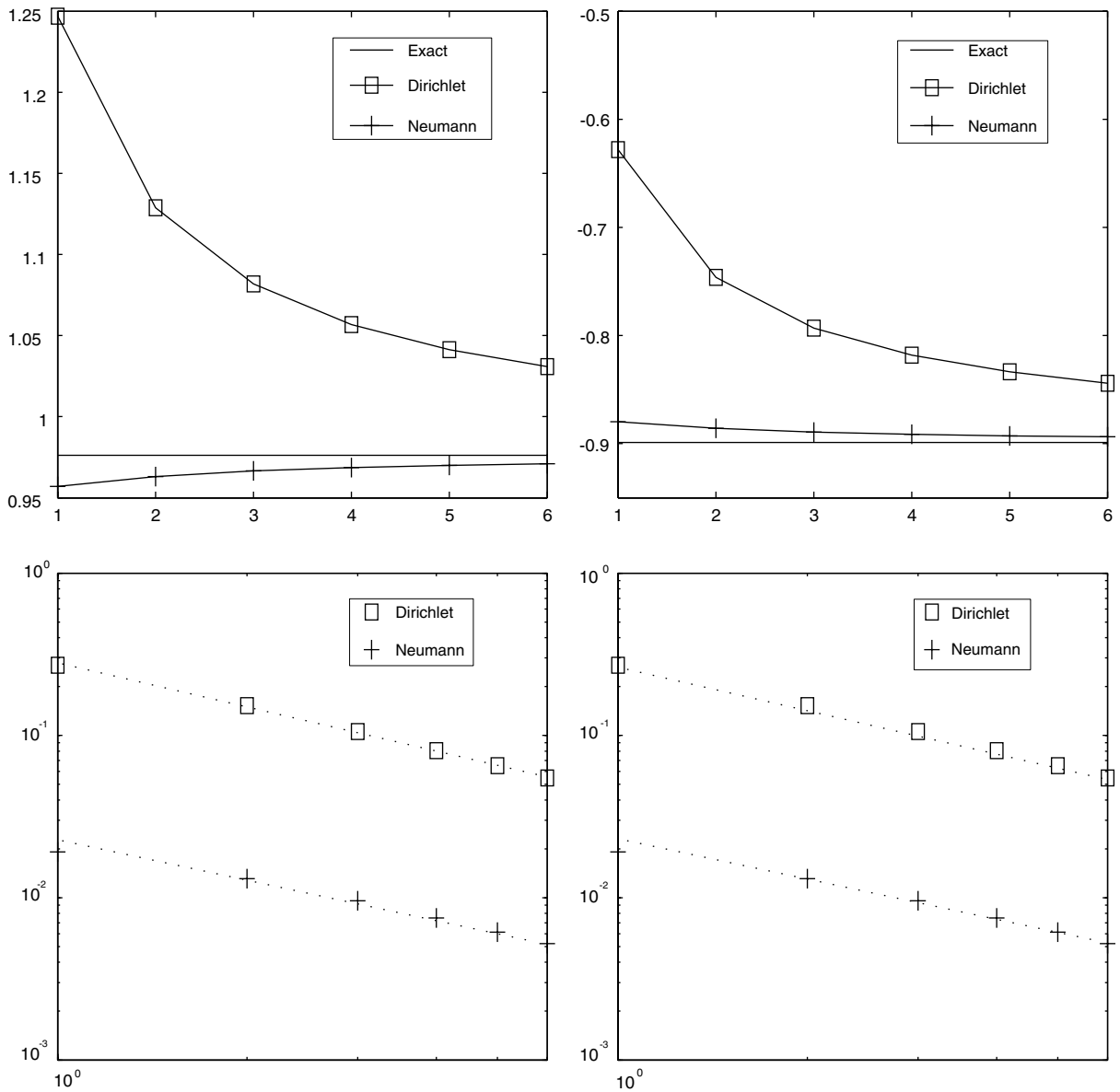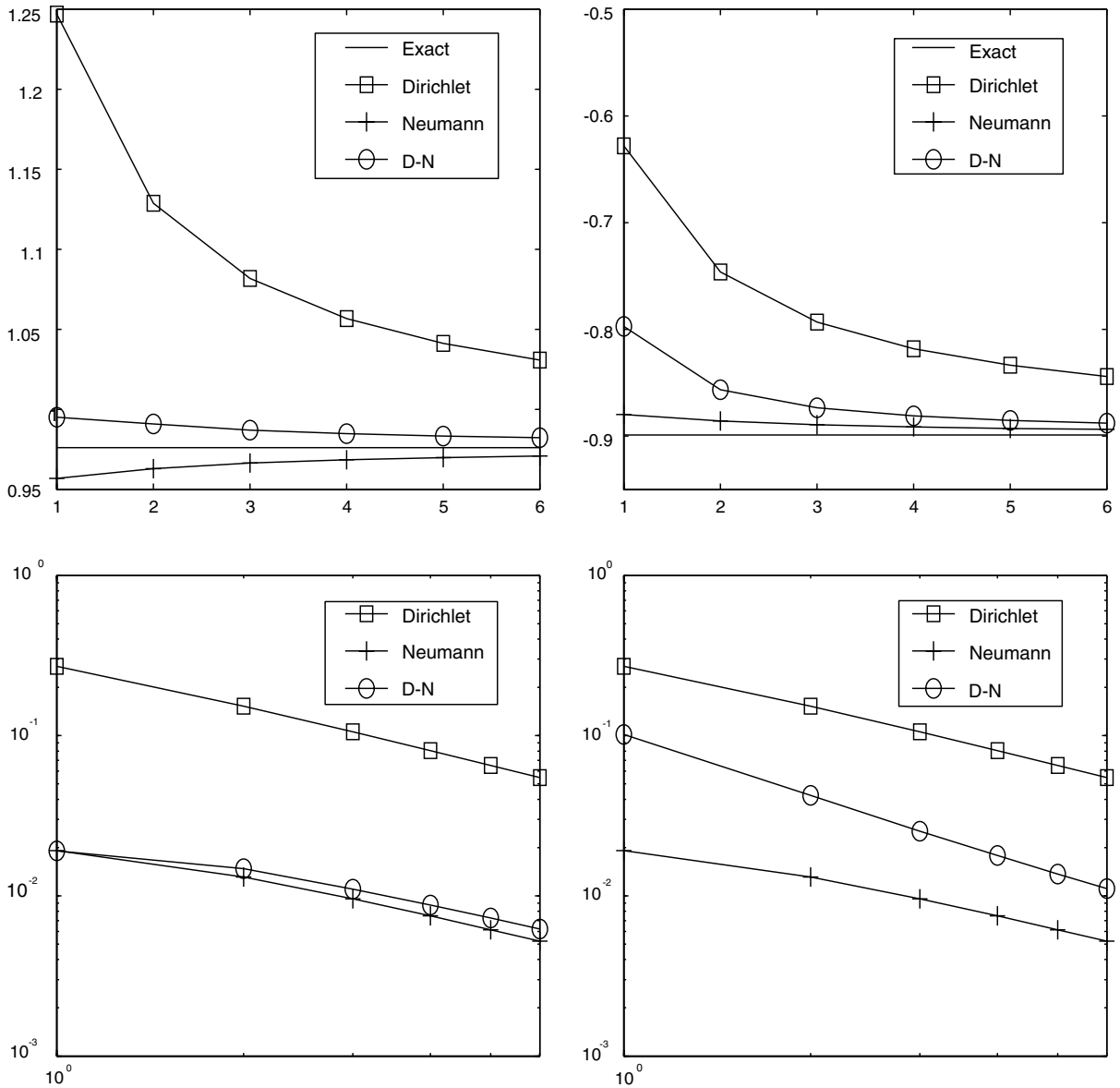
Fig. 10. Periodic laminated media – effective coefficients $k_{11}^* = k_{22}^*$ and $k_{12}^* = k_{21}^*$ (upper-right) vs. cell-size; error of $k_{11}^* = k_{22}^*$ (lower-left) and $k_{12}^* = k_{21}^*$ (lower-right). The slopes of the dotted lines are approximately -1.0.

take that into account, we should modify (3.7) and (3.8) to (this has been noted in the literature, see for example [12,11])

$$\langle k^\varepsilon(\mathbf{x})\nabla u_1 \rangle = K_{dn}^* \langle \nabla u_1 \rangle, \tag{3.9}$$
$$\langle k^\varepsilon(\mathbf{x})\nabla u_2 \rangle = K_{dn}^* \langle \nabla u_2 \rangle. \tag{3.10}$$

The results using this modified definition is depicted in Fig. 11. It can be seen that using the D–N formulation effective tensor is strictly between the results of the Dirichlet and Neumann formulations. This is easily proved along the lines in the proof of Theorem 2.1.

This example clearly shows the advantage of using systematic procedures and formulations, as is advocated in HMM. Indeed using the HMM framework, mistakes such as the ones in (3.7) and (3.8) are automatically avoided.

Table 2
Periodic laminated media – average gradient of u_1 in (3.5): $\langle \nabla u_1 \rangle = (\langle \partial_{x_1} u_1 \rangle, \langle \partial_{x_2} u_1 \rangle)^{\mathrm{T}}$ vs. cell size L

L	1	2	3	4	5	6
$\langle \partial_{x_1} u_1 \rangle$	1.0	1.0	1.0	1.0	1.0	1.0
$\langle \partial_{x_2} u_1 \rangle$	0.6435	0.6389	0.6453	0.6492	0.6517	0.6532

Fig. 11. Periodic laminated media – effective coefficient $k_{11}^* = k_{22}^*$ (upper-left) $k_{12}^* = k_{21}^*$ (upper-right) vs. cell size; error of $k_{11}^* = k_{22}^*$ (lower-left) $k_{12}^* = k_{21}^*$ (lower-right) vs. cell size.

4. Effects of different averaging methods

Finally, we study the effects of using alternative averaging procedures. We will discuss only the case with periodic microstructure since the conclusions for the random problems are quite similar.

We compare three different averaging procedures: direct averaging over the whole domain, weighted averaging and truncated averaging. Figs. 12–14 show the results for the periodic problem with coefficient (3.1). We see clearly that the weighted and truncated averages produce better results for the Dirichlet formulation. The results for the Neumann formulation is mixed. There are improvements but in some cases the improvement is quite small. This is also consistent with our intuition: in general we expected the Dirichlet boundary condition to be the hardest boundary condition, and therefore introduces most boundary effects. These boundary effects
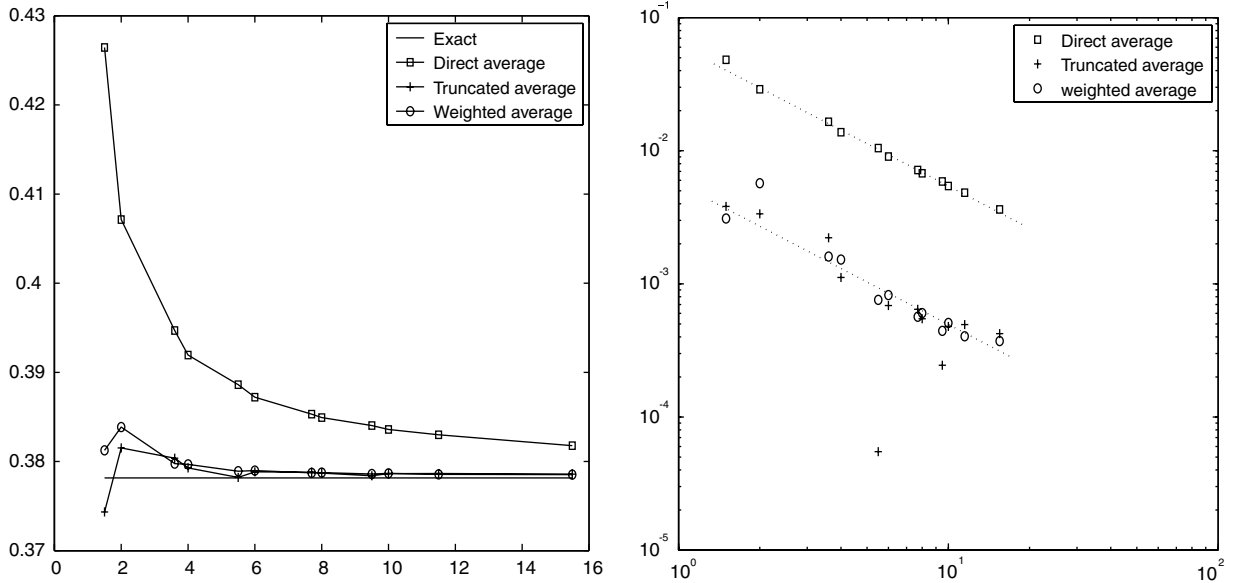

Fig. 12. Effective of different averaging procedure for the example (3.1) with Dirichlet formulation. Effective coefficient obtained by different average procedures vs. cell size (left); log–log plot of the absolute error vs. cell size (right). The slope of the upper dotted line is −1.05, and the slope of the lower dotted line is −1.00.
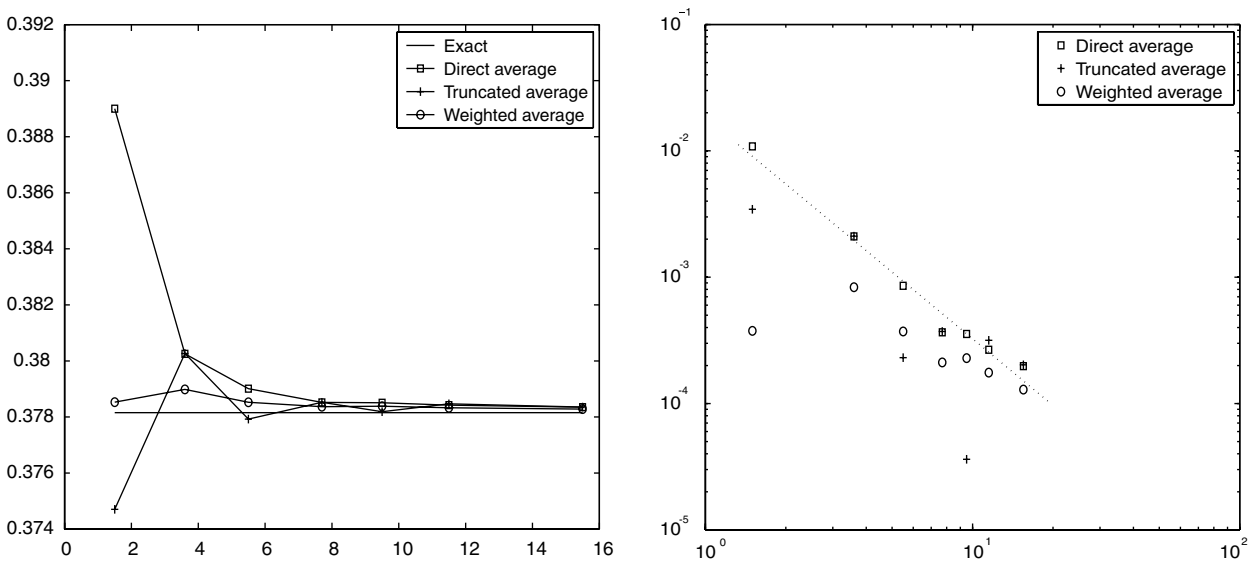

Fig. 13. Same as in Fig. 12, but with periodic formulation. The slope of the dotted line is −1.50.
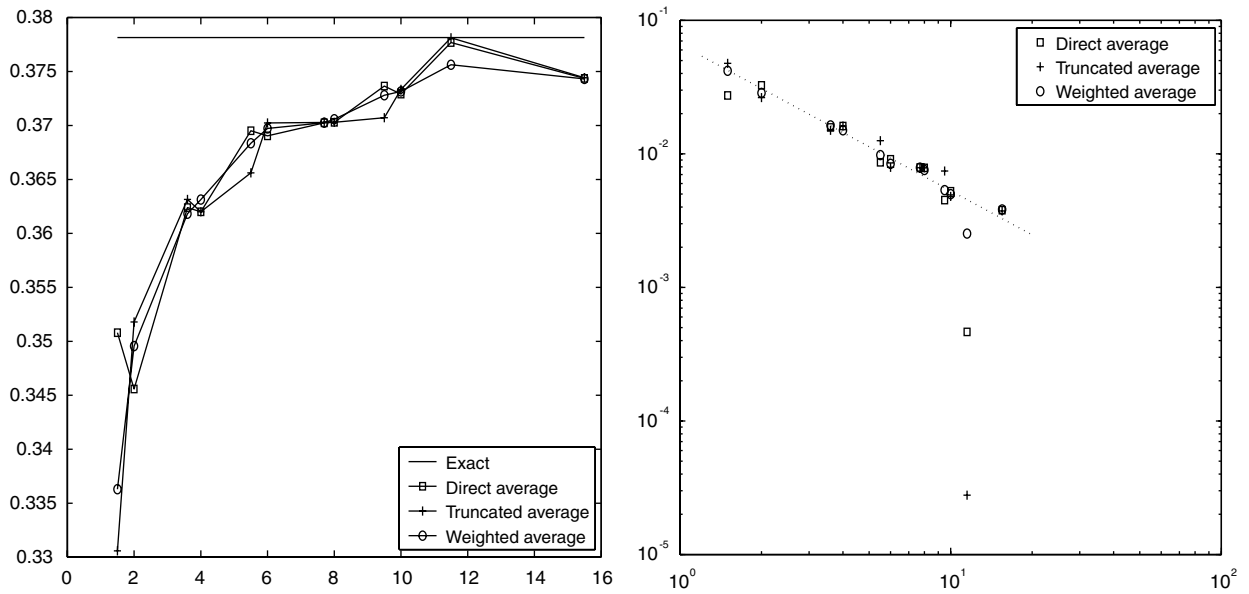
Fig. 14. Same as in Fig. 12, but with Neumann formulation. The slope of the dotted line is −1.07.

are corrected using weighted or truncated averages. We also expect periodic and Neumann boundary conditions to be much softer and introduce less boundary effects.

5. Conclusions

Following conclusions can be drawn from this work:

1. Periodic boundary condition performs better for both the random and periodic problems.
2. The variance of the estimated effective tensor behaves as $\sigma^2 \sim L^{-d}$ for random check-board problem in $\mathbb{R}^d$, and $\sigma^2 \sim L^{-2}$ for the periodic problem.
3. In general Neumann formulation underestimates the effective tensor and Dirichlet formulation overestimates the effective tensor. In both cases, the effective conductivity tensors converge to the infinite volume limit with first order accuracy $O(1/L)$, where L is the cell size.
4. Weighted or truncated averaging improve the accuracy for the Dirichlet formulation. It has little effect for the periodic formulation. For the Neumann formulation, it improves the accuracy in some cases. In general, the results of the weighted averaging are more robust.

Acknowledgements

References

[1] F.F. Abraham, J.Q. Broughton, N. Bernstein, E. Kaxiras, Concurrent coupling of length scales: Methodology and application, Phys. Rev. B 60 (1999) 2391–2402.
[2] J. Bear, Dynamics of Fluids in Porous Media, American Elsevier, New York, 1972.

[3] A. Bourgeat, A. Piatnitski, Approximations of effective coefficients in stochastic homogenization, Ann. Inst. H. Poincaré Probab. Stat. 40 (2004) 153–165.

[4] L.J. Durlofsky, Numerical-calculation of equivalent grid block permeability tensors for heterogeous porous media, Water Resour. Res. 27 (1991) 699–708.

[5] W. E, B. Engquist, The heterogeneous multiscale methods, Commun. Math. Sci. 1 (2003) 87–132.

[6] W. E, B. Engquist, X. Li, W. Ren, E. Vanden-Eijnden, The heterogeneous multiscale method: a review, 2005. Available from (http://www.math.princeton.edu/multiscale).

[7] W. E, P. Ming, P. Zhang, Analysis of the heterogeneous multiscale method for elliptic homogenization problems, J. Am. Math. Soc. 18 (2005) 121–156.

[8] G.C. Papanicolaou, S.R.S. Varadhan, Boundary value problems with rapidly oscillating random coefficients, in: J. Fritz et al. (Eds.), Random Fields, 27, North-Holland, Amsterdam, 1981, pp. 835–873.

[9] S. Pecullan, L.V. Gibiansky, S. Torquato, Scale effects on the elastic behavior of periodic and hierarchical two-dimensional composites, J. Mech. Phys. Solids 47 (1999) 1509–1542.

[10] S. Torquato, Random Heterogeneous Materials: Microstructure and Macroscopic Properties, Springer Verlag, 2001.

[11] X.H. Wen, L.J. Durlofsky, M.G. Edwards, Use of border regions for improved permeability upscaling, Math. Geol. 35 (2003) 521–547.

[12] X.H. Wu, Y.R. Efendiev, T.Y. Hou, Analysis of upscaling absolute permeability, Discret. Contin. Dyn. Systems, Ser. B 2 (2002) 185–204.

[13] V.V. Zhikov, S.M. Kozlov, O.A. Oleinik, Homogenization of Differential Operators and Integral Functionals, Springer verlag, Berlin Heidelberg, 1994.